Report No.
UCB/SEMM-2011/09

Structural Engineering
Mechanics and Materials

# EARTHQUAKE RESISTANT AND RESILIENT TALL REINFORCED CONCRETE BUILDINGS USING BASE ISOLATION AND ROCKING CORE-WALLS

By

Vladimir Calugaru and Marios Panagiotou

December 2011

Department of Civil and Environmental Engineering
University of California, Berkeley

# Earthquake-Resistant and Resilient Tall Reinforced Concrete Buildings Using Base Isolation and Rocking Core-Walls

Vladimir Calugaru and Marios Panagiotou
*Department of Civil and Environmental Engineering, University of California, Berkeley, CA, USA*

SUMMARY

This report investigates numerically the use of seismic isolation and/or rocking core-walls to improve the seismic performance of tall buildings with a reinforced concrete core-wall as the main lateral force resisting element above the ground level. Five 20-story tall reinforced concrete core-wall buildings were considered. The first two buildings are conventionally designed to accommodate the majority of inelastic deformations in a single flexural plastic hinge at the ground level of the core-walls. The third building uses an isolation plane, consisting of elastomeric bearings and viscous dampers at the base of the building, below the ground level. The fourth building uses a core-wall, designed to rock at the ground level. The last building uses both the isolation plane and the rocking core-wall of the third and fourth building, respectively. The rocking core-wall design uses a newly proposed armored core-wall with externally attached buckling restrained braces and viscous dampers. The buildings are subjected to 14 strong pulse-type near-fault ground motions. The response is presented in terms of floor accelerations, forces, displacements, material strains, as well as deformations and stresses of the bearings. In comparison with conventionally designed buildings, the building with a single base isolation plane did not prevent the formation of a plastic hinge at the core-wall, while the building designed with a rocking core-wall did not reduce floor accelerations and forces. The building with both the base isolation plane and the rocking core-wall demonstrated superior performance, significantly reducing floor accelerations, forces, and preventing the formation of a plastic hinge at the core-wall, concentrating plastic deformation in external elements that can be easily repaired or replaced.

## 1 INTRODUCTION

Construction of buildings taller than 50 m in the United States (U.S.) and around the world is increasing due to the rapid growth of cities and their dense inner cores [1]. This trend has been slower in regions of high seismicity, but numerous tall buildings are being planned or designed in regions vulnerable to earthquakes.

Considerable damage to tall buildings due to earthquakes has a decades-old history. Outside the U.S. in the 1985 M8.0 Mexico earthquake, which caused around 10,000 fatalities, at least 15 tall buildings (14 to 18-stories tall) at a distance of 350 km from the epicenter suffered major damage or collapsed in Mexico City due to amplification of the long-period content of the ground motions by deep and soft soil deposits [2]. In the 1995 M6.9 Kobe, Japan, earthquake, 40% of the 10 to 12 stories buildings were heavily damaged or collapsed [2]. In the 1999 M7.6 Chi-Chi, Taiwan, earthquake more than twenty-five 10 to 20-story reinforced concrete (RC) frame buildings collapsed [3]. In the recent 2010 M8.8 Chile earthquake, one 15-story tall building collapsed, a 21-story tall building partially collapsed, see Figure 1, and at least 15 other buildings between 12- and 23-stories tall suffered significant, and in some cases irreparable, damage [4-7]. Finally during the very recent M6.3 2011 Christchurch, New Zealand, earthquake, the tallest structure in the city, a 26-story tall hotel, experienced significant damage, and large permanent tilt of the building [8] that had to be demolished. The damage of tall buildings in the Chile and New Zealand earthquakes was due to a combination of deficiencies in the structural design and detailing and strong ground motions [4, 5] with characteristics that significantly excited these structures. Commercial and residential buildings in the immediate shade of heavily damaged tall buildings have to be evacuated until the damaged buildings are successfully demolished, which can be problematic as demolition of damaged buildings is much more complicated compared to those that are in sound condition. In the U.S. during the last

forty years, the 1971 M6.6 San Fernando, the 1989 M6.9 Loma Prieta, and the 1994 M6.7 Northridge earthquakes resulted in the most damage to infrastructure, with the largest number of fatalities equal to 65, 63, and 60, respectively [9]. In the Loma Prieta earthquake, the major cities of San Francisco and Oakland were at considerable distance from the epicenter (~100 km), resulting in low excitation and almost no damage to tall buildings [10, 11]. In the case of the San Fernando and Northridge earthquakes, a combination of the relatively large distance of the epicenter from downtown Los Angeles (35 and 31 km, respectively), and minor fault rupture directivity, for downtown Los Angeles, resulted in moderate excitation and minor damage of tall buildings in downtown Los Angeles [12,13].

Figure 1. Partially collapsed O'Higgins building threatens the surrounding built environment. This building, the tallest building in Conception, suffered significant damage from the 2010 M8.8 Chile earthquake (photo courtesy of J. Restrepo).

Current codes [14] have been calibrated for low- or moderate-rise construction using standard construction materials and without regard to post-earthquake damage, economic losses, and reparability. This is becoming a major concern in the seismic design of tall buildings—particularly those using high-performance materials and employing nonconforming structural systems and details—which may not achieve performance expectations [15]. *Ad hoc* procedures have been developed by several groups on minimum performance expectations, design, and analysis requirements, and to streamline performance-based seismic assessment of tall buildings as they are currently designed [16-19]. None of these guidelines address how to enhance the seismic resilience of tall buildings to reduce post-earthquake damage.

Many tall buildings in highly seismic regions are now designed with RC core-walls as the main lateral force resisting system. Based on current practice, RC core-wall buildings are designed to develop nonlinear deformations in regions defined as plastic hinges located at the base of the core-walls [19-21]. Numerical studies have shown that tall buildings undergo strong pulse-type near-fault ground shaking they experience significant inelastic deformations [21, 22] and thus significant post-earthquake damage. At best required repairs of this damage may be expensive, time consuming, and disruptive. In addition when excited with motions that contain pulses of predominant period in the range of the second modal period, these buildings develop high acceleration and force demands along their entire height with significant contribution from the second and higher modes of response [21, 22]. For walls designed to restrict all the inelastic deformations in a single plastic hinge at their base, studies have shown that large bending moment demands develop around mid-height and a large amount of longitudinal reinforcement is required for elastic response of these regions [21, 22]. To avoid the development of large bending moments on the upper part of the wall some designs allow plasticity to develop anywhere along the height of the wall which requires special detailing over the entire wall height in order for these regions to be able to accommodate possible inelastic deformations [21]. To reduce second and higher modes of response as well as transverse reinforcement requirements along the height of the walls Panagiotou and Restrepo [21] proposed a design concept with two flexural plastic hinges, one at the base and another at the mid-height of the

wall in this type of buildings. Munir and Warnitchai [23] proposed a design with multiple plastic hinges along the height of the wall. Although effective to a certain extent these designs cannot eliminate post-earthquake damage associated with plastic hinging.

Consideration of using seismic isolation to reduce demands and post-earthquake damage in tall buildings is proposed herein. Traditionally, seismic isolation has been considered most effective for relatively short and stiff structures by elongating their fundamental period, thus reducing the accelerations and forces they develop. For tall buildings the main goal of seismic isolation is not to increase the already long fundamental period. Instead, it concentrates deformations in a few robust locations that are easily replaceable, as well as to reduce the contribution of higher modes in response and the corresponding structural demands (accelerations, forces, and displacements) that may cause structural and nonstructural damage.

Japan is currently the leading proponent of applying seismic isolation in tall buildings [24-25]. Forty percent of all recorded isolated buildings built in Japan after 1995 had a height to plan view length ratio larger than two [24] with the tallest being 41-stories [26]. Incorporating isolation in the upper part of buildings has been also proposed or used [27-32]. Large elastomeric bearings, e.g. with 1.5 m diameter, required to isolate tall buildings are currently available [33] and they have been studied experimentally under combined lateral and vertical loading [34-36]. Large friction bearings also exist [37, 38].

Another strategy, which has been studied numerically, to reduce post-earthquake damage due to plastic hinging in tall RC wall buildings is to use rocking walls under gravity [39], or rocking walls that use unbonded steel and post-tensioning tendons [40]. The latter study proposed a design including multiple rocking planes along the height of a wall to reduce the contribution of second and higher modes of response. The combination of base isolation and rocking has been investigated numerically for a rigid block subjected to pulse-type ground excitations [41].

This report investigates numerically the use of seismic isolation and/or rocking core-walls to improve the seismic performance of tall buildings with a RC core-wall as the main lateral force resisting element above the ground level. A new design concept of a RC rocking core-wall cast in a steel shell over the first story height is proposed.

## 2 DESCRIPTION AND DESIGN OF BUILDINGS

Five 20-story buildings were considered. A RC core-wall coupled with a gravity system provided the lateral force resistance above the ground level, see
Figure 2. Common to all buildings in this study, the core wall was 7.9 m long and 0.46 m thick.

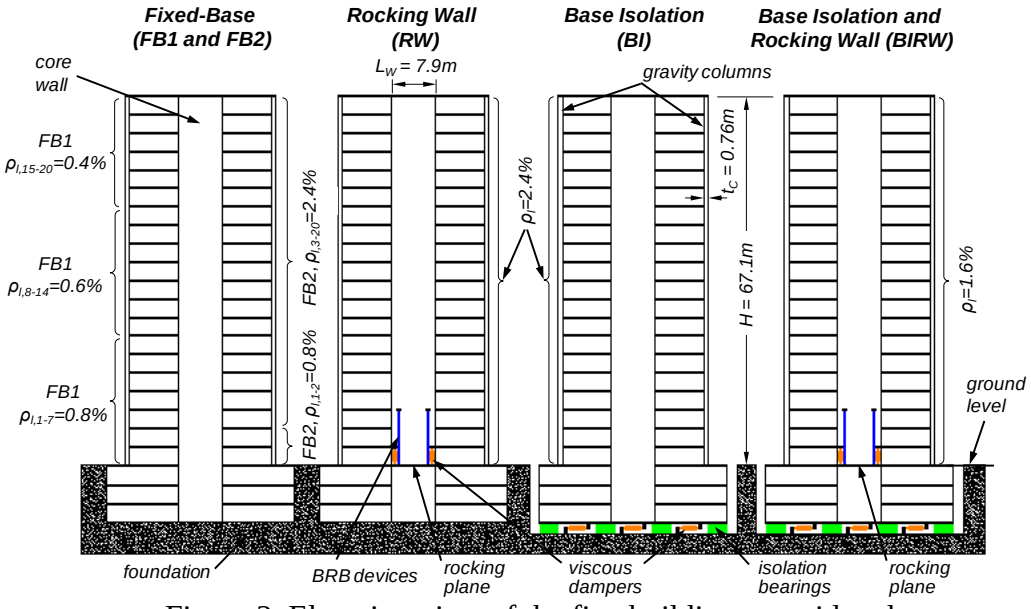

Figure 2. Elevation view of the five buildings considered.

**Error! Reference source not found.**(a) shows the common floor plan view of the buildings above ground. The gravity system was common to all buildings consisting of 0.76-m × 0.76-m columns and 0.2-m-thick slabs. The longitudinal steel ratio of the columns was 1.0%. The slab reinforcement consisted of #5 bars at 0.3 m spacing in the two directions, both top and bottom. The five buildings differ in the locations where the majority of deformations are designed to develop. The first two are conventional designs based on current practice where the wall is assumed fixed at the ground level, see
Figure 2. The third building used one isolation plane below ground. The fourth considered a core-wall designed to rock at the ground level, and the fifth incorporates both the isolation plane and the rocking core-wall of the third and fourth building, respectively. Table 1 lists the main characteristics of the buildings. For all buildings, concrete of $f_c^{'}$ = 48 MPa compressive strength was considered for all members. The following sections describe the five designs.

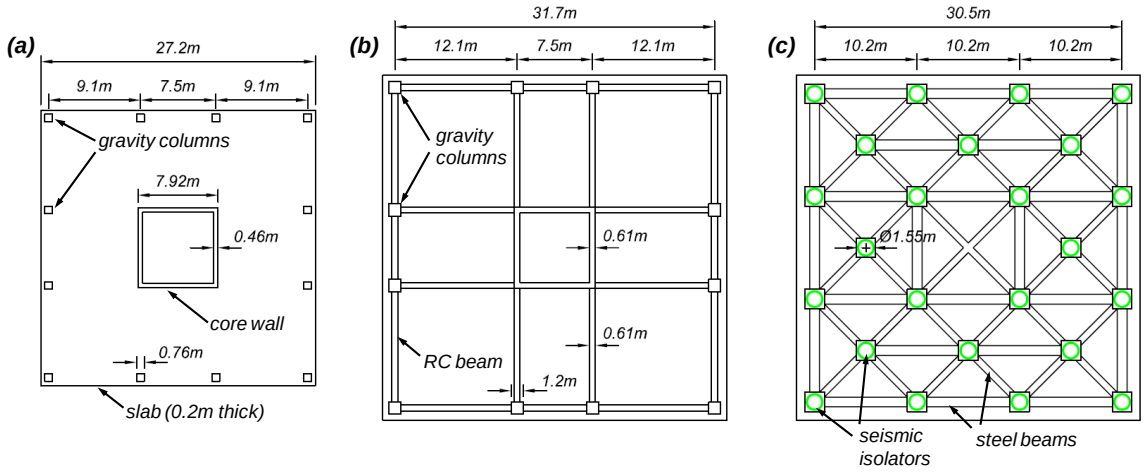


Figure 3. Plan view of: (a) floor above ground, (b) floor below ground, and (c) isolation plane.

Table 1. Building characteristics.

| | Fixed Base 1 (FB1) | Fixed Base 2 (FB2) | Base Isolated (BI) | Rocking Wall (RW) | BI and RW (BIRW) |
|---|---|---|---|---|---|
| Axial load ratio at theground level of the core-wall due to gravity $P_{cw} / (f'_c A_g)$ | | | 0.09 | | |
| Seismic weight, above ground floor, $w$ (kN) | | | 7123 | | |
| Seismic weight, underground floor, $w_{ug}$ (kN) | - | - | - | 10685 | 10685 |
| Expected flexural strength at ground level of wall, $M_{b,y}$ (kN·m) | 501403 | 501403 | 340972 | 850170 | 340972 |
| Bonded steel in stories 3 – 20, $\rho_{l,3\text{-}20}$ (%) | 0.8 | 2.4 | 2.4 | 2.4 | 1.6 |
| Bonded steel in stories 1 and 2, $\rho_{l,1\text{-}2}$ (%) | 0.8 | 0.8 | 2.4 | 2.4 | 1.6 |
| Number of BRBs ($F_y$ = 4661 kN) and equivalent steel ratio, $\rho_{UB}$ (%) in parenthesis | - | - | 8 (0.6) | - | 8 (0.6) |
| Number of bearings ($D$=1.55m, $t_r$ =0.38m) | - | - | - | 24 | 24 |
| Number of horizontal dampers (1500 kN, $\alpha$=0.7) | - | - | - | 12 | 12 |
| Number of vertical dampers (2000 kN, $\alpha$=0.7) | - | - | 8 | - | 8 |

2.1 *Fixed-base buildings (FB1 and FB2)*

In these designs, the majority of inelastic deformations developed in a flexural plastic hinge at the ground level of the core-wall. Modal response spectrum analysis (MRSA), based on the requirements of ASCE-7 [42], with a response modification factor of $R$ = 5, was used to obtain design forces for the fixed-base buildings for a site in downtown Pasadena, California, for soil type C, corresponding to very dense soil and soft rock. Figure 4 depicts the design basis earthquake (DBE) and maximum considered earthquake (MCE) acceleration and displacement spectra for the site considered. An effective section moment of inertia $I_e = 0.5I_g$ recommended by FEMA 356 [43] was used for the core-walls along their entire height for the MRSA where $I_g$ is the gross section moment of inertia of the core-wall.

The design bending moment, $M_u$, and shear force, $V_u$, envelopes are shown in Figure 5, where the MRSA bending moment and shear force envelopes are labeled *MRSA*. The $MRSA_{Mb,o}$ envelopes, shown also in Figure 5, are the *MRSA* envelopes scaled by $1.25M_{b,y}/M_{b,MRSA}$, where 1.25 is the base flexural overstrength factor, $M_{b,MRSA}$ is the *MRSA* base bending moment, and $M_{b,y}$ the expected flexural strength at the ground level of the wall computed by moment-curvature analysis and reported in Figure 3. Plan view of: (a) floor above ground, (b) floor below ground, and (c) isolation plane.

Table 1.

In the first considered fixed-base design (FB1) plasticity is allowed to develop in any region along the height of the wall. The longitudinal steel ratios, $\rho_l$, in the bottom, middle, and top thirds of the wall were 0.8%, 0.6%, and 0.4%, respectively.

The second fixed-base building (FB2) was designed to form a single flexural plastic hinge extending over the bottom two stories of the building, see Figure 2. The reinforcing steel ratio in the plastic hinge region was $\rho_{l,1\text{-}2}$ = 0.8%. A high longitudinal steel ratio $\rho_{l,3\text{-}20}$ = 2.4% above the plastic hinge was provided to ensure elastic response of this part of the wall. These two designs assume that adequate transverse and confinement reinforcement is provided along the height of the wall to ensure the development of inelastic deformations without strength degradation.

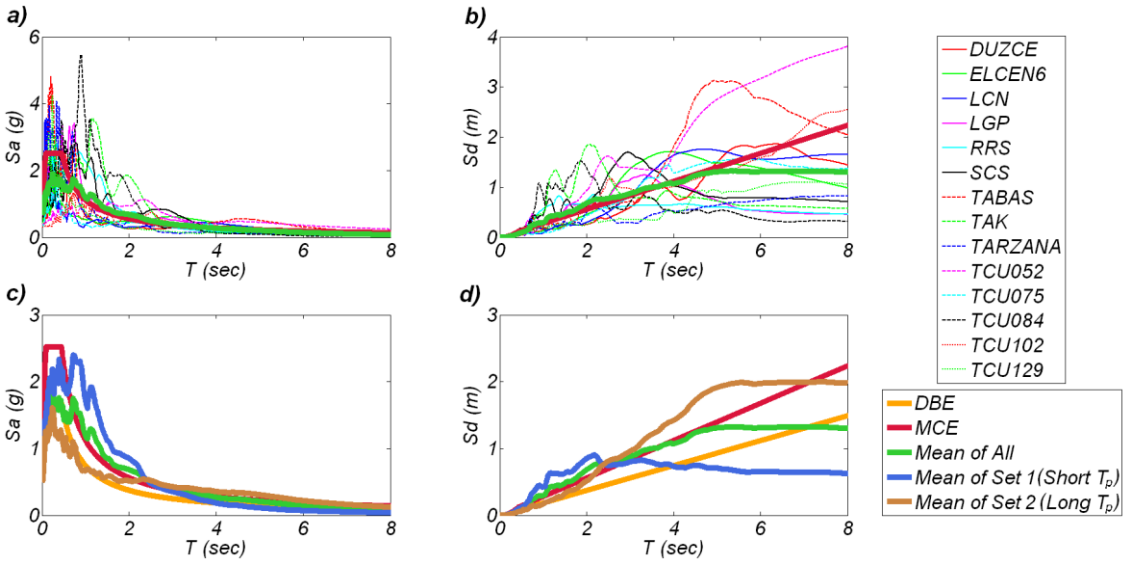


Figure 4. Absolute acceleration and relative displacement response spectra of the 14 considered ground motions, and mean response spectra for 2% damping, as well as DBE- and MCE-level design spectra.

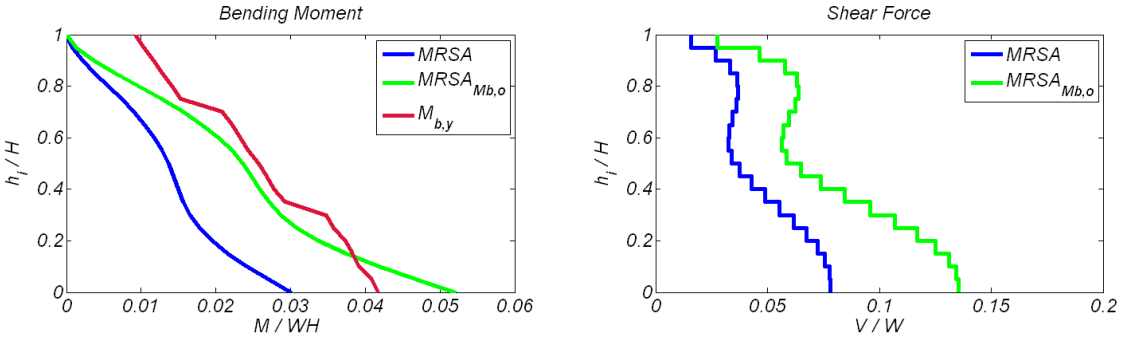

Figure 5. Design envelopes calculated with MRSA for the fixed-base buildings.

## 2.2 *Base-isolated (BI) building*

The third design, referred to as BI, used a single isolation plane consisting of 24 low-damping laminated elastomeric bearings, and twelve dampers, each with 1500 kN force and 0.6m stroke capacity. This isolation plane was located at the base of the building below ground to achieve the maximum plan view length and ensure that the bearings did not experience tension. The force-displacement behavior of these bearings was linear elastic.

The main objective of this design was to eliminate the inelastic response at the base of the wall, and reduce floor accelerations and forces without exceeding the capacity of the bearings under significant lateral deformation and concurrent vertical load. To achieve the latter, the stiffness and thus the period of the building needs to be controlled to avoid large displacements associated with strong low-frequency excitation.

Aiming at large deformation capacity, the bearings had a diameter D = 1.55 m and a displacement capacity $\Delta_{b,u}$ = 0.9 m, corresponding to $\Delta_{b,u}$ / D = 0.6. The total height of rubber, and of the bearing was $t_r$ = 0. 38m, and $H_b$ = 0.44 m, respectively. For these properties and a rubber shear modulus $G_r$ = 483 kPa, the lateral, vertical (compression), and rotational stiffnesses of each bearing were $K_h$ = 2392 kN / m, $K_v$ = 6661 MN / m, and $K_\theta$ = 104320 MN / rad, respectively. Bearings with these dimensions and properties are commercially available and their behavior has been verified experimentally [33]. The compressive stress due to gravity of the bearings was 4.1 MPa.

To prevent the formation of a plastic hinge at core-wall at the ground level, the core-wall was heavily reinforced with $\rho_l$ = 2.4%. Based on a pushover analysis using the first mode lateral force profile, the displacement of the bearings and the roof displacement at which the tensile strain of steel at the base of the wall was 0.5%, were calculated to be equal to 0.52 m, and 1.08 m, respectively. At this level of displacement the ratio of the shear force at the ground level to the total seismic weight was computed to be $V / W_t$ = 0.1. As shown in Figure 4 at the first mode period $T_{l,1}$ = 3.8 sec the elastic spectral displacement demand for the MCE level was equal to 1.3 m. Thus, yielding of the wall at the ground level was expected for motions with elastic displacement demand close or higher than the MCE spectrum in this period range. The dampers were designed to result in a peak horizontal damping force of 10% of the total building weight. The case of reducing the stiffness of the isolation plane and thus increasing the period of the building was investigated, see Section 5.6, but this proved inadequate. Despite the smaller stiffness, the development of larger bearing displacements resulted in a similar level of lateral forces, and similarly when the stiffness of the isolation plane was increased. In this case, the smaller developed displacements of the bearings in combination with the larger stiffness of the isolation plane resulted in similar level of lateral forces.

The stability of the bearings under peak expected displacement equal to 0.7 m and concurrent peak vertical compressive stress of 8.2 MPa was checked [33, 50] and was found to be adequate.

A small amount of lead plug can be used in the bearings to increase their initial stiffness and control deformations under wind loads. This small amount of lead plug will have negligible effect on the developed seismic displacements of the bearings.

2.3 *Rocking wall (RW) building*

In contrast with the FB1 and FB2 buildings, the RW building used a rocking core-wall designed to rock at the ground level to avoid the formation of a flexural plastic hinge at the base of the wall. Due to the significant contribution of the axial load in moment resistance of the core-wall, post-tension was not required to achieve re-centering behavior. To maximize the confinement of the concrete of the core and eliminate strength and stiffness degradation associated with damage of the concrete in compression during rocking about the compression toe, an armored rocking core-wall system was considered. The term "armored" is used because the core wall at its base is cast into a 0.025-m-thick steel shell, see Figure 6, that serves as a stay-in-place form in the entire first story. The cross-connected steel shell encloses the entire core, providing excellent confinement for any possible angle of attack of the earthquake excitation. To enhance constructability, structural integrity, and performance, threaded rods were used in the two directions of the core-wall section plane to cross-connect the steel shell. The steel shell results in a volumetric confinement ratio in the direction parallel to wall thickness $\rho_v$ = 11%. The $M_{b,y}$ reported in Figure 3. Plan view of: (a) floor above ground, (b) floor below ground, and (c) isolation plane.

Table 1 for the RW building is at first yield of the outer BRB.

To further enhance the behavior of the core wall in compression, T-headed bars were considered as bonded reinforcement at the base of the core wall (not shown in Figure 6 for clarity). With the head at the interface with the wall, twin T-headed bars were used at the top of the foundation, improving the compression force transfer to the foundation, see Figure 7. Use of headed bars or bars welded on steel plates has been verified with experimental work by different researchers [44, 45]. For protection against sliding, steel shear keys can be used at the corners of the core-wall in both directions. A number of passive methods can be used to enhance the sliding resistance of the wall at its base [46, 47].

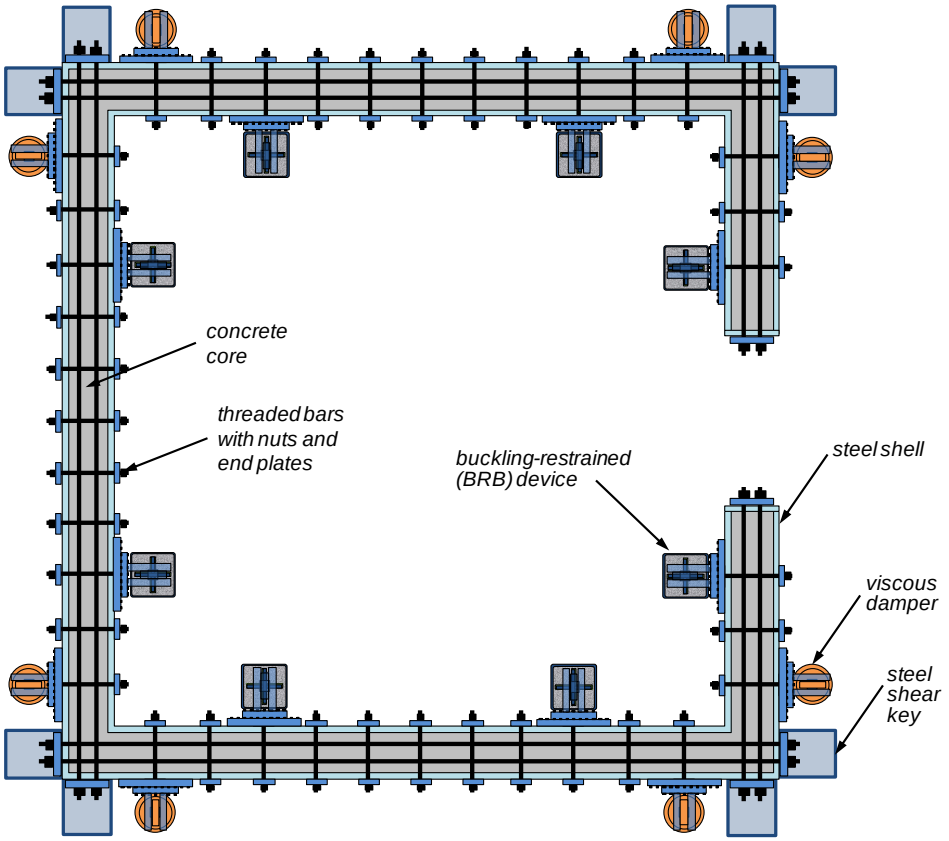

Figure 6. Section view of armored core-wall.

Buckling restrained hysteretic devices, e.g. buckling restrained braces (BRB), were fastened externally to the core wall to provide hysteretic energy dissipation to the rocking plane. The length of the hysteretic devices was selected to result in an accepted level of inelastic strains for the maximum expected deformations of the wall. Eight BRB devices, 9 m long with a yield force $F_y$ = 4661 kN each, were externally attached to the core wall. The yield length of the BRBs was 6 m corresponding to 0.24 m of elongation for 4% tensile strain. The accumulated yield force of the BRBs is equivalent to that provided by a 0.6% ratio of longitudinal reinforcement in the core-wall, see Figure 3. Plan view of: (a) floor above ground, (b) floor below ground, and (c) isolation plane.

Table 1. The BRBs were placed on the inner side of the core wall to avoid the development of compressive strains as well as to reduce their peak tensile strain. Large BRBs (6 m long) of similar yield force capacity (4500 kN) have been tested and have been proven to be able to develop tensile strains larger than 3.5% [48]. Alternatively, unbonded reinforcement can be detailed within the core-wall. The disadvantage of the system with internal unbonded reinforcement is that it does not allow for post-earthquake inspection and replacement. The BRB system is externally attached to the wall, and thus can be easily inspected and replaced, resulting in a system that is adaptable over the service life of the building. Rocking walls for medium-rise structures with externally fastened hysteretic and viscous devices have been tested experimentally [47].

In addition to the eight BRBs, eight 2000 kN viscous dampers with 0.6 m stroke were used in the vertical direction. Dampers with such characteristics are commercially available and have been used in various structures [49]. These dampers can provide additional energy dissipation to the BRBs and reduce effects due to impact of the core-wall. The accumulated force of the eight dampers was selected to correspond to 42% of the total yield force due to the BRBs. Section 5.4 discusses variations of this design, considering either the BRBs, the viscous dampers, or none of them.

The design objectives were as follows: (i) ensure that the gravity load is enough to re-center the core-wall after reaching its ultimate roof lateral displacement; (ii) to limit the peak compressive strain of concrete to less than 1.5%; and (iii) to limit the peak tensile strain in the unbonded reinforcement to 4%. At ultimate roof displacement of 2.0 m corresponding to a 3% roof drift ratio, the neutral axis depth was computed to be $0.07L_w$ (using the first mode lateral force profile) and the peak compressive strain to be 0.8%, while the strain of the unbonded steel was equal to 2.8%. At this instant the uplift of the wall was equal to 0.21 m.

### 2.4 *Building with base isolation and rocking wall (BIRW)*

The BIRW design uses both the isolation plane and the rocking core-wall of the BI and RW buildings, respectively. This design combines the beneficial features of the BI design—by controlling the force and deformation at the isolation plane below ground by reducing second and higher modes—as well as the benefits of the RW—avoiding the formation of a flexural plastic hinge at the ground level of the wall. Here, deformations are distributed between the displacement of the bearings, the rotation of the wall at the rocking plane, and the elastic deformations of the core-wall above the rocking plane, see Figure 7. In this design, horizontal dampers were used at the base isolation plane identical to those used in the BI building. Based on a monotonic static analysis, using the first model lateral force profile, when the relative to the ground level displacement at the roof of the building was 2 m corresponding to 3% drift ratio (relative to the ground level) the shear force of the wall at the ground level to the total seismic weight of the building was $V / W_t$ = 0.05. At the same instant, the displacement of the base isolation plane below the ground level was 0.15 m.

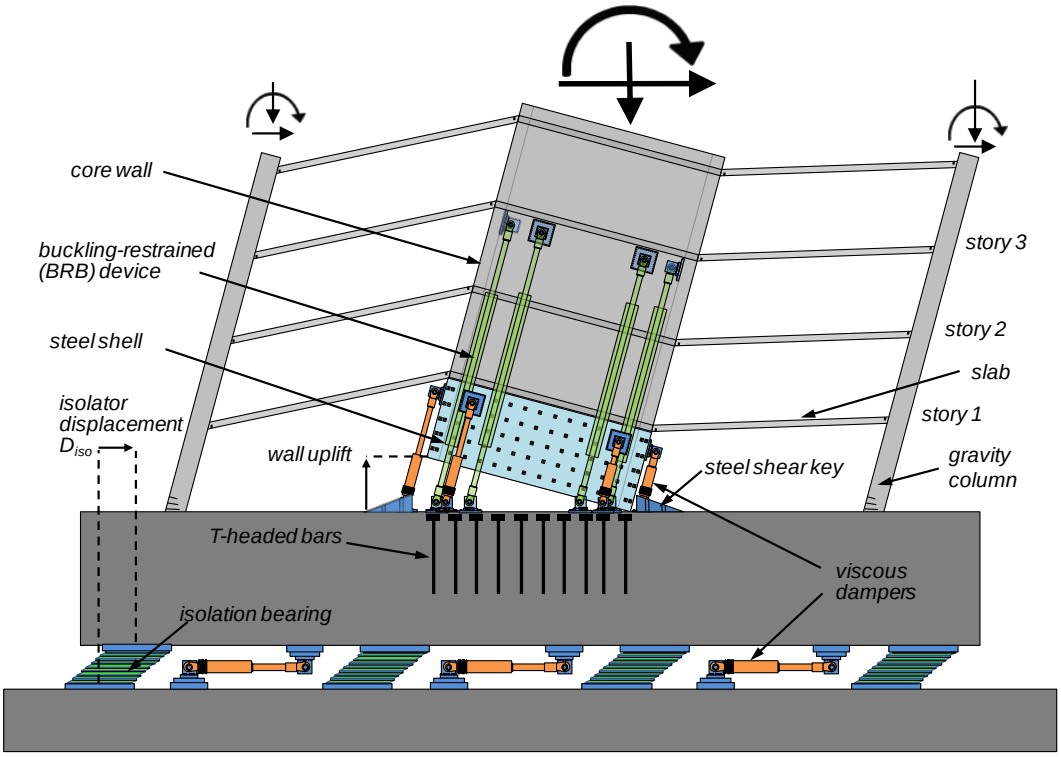


Figure 7. Base isolation and rocking planes of BIRW building in an exaggerated deformed state.

## 3 NUMERICAL MODELING

The Open System for Earthquake Engineering Simulation (OpenSees) software [51] was used in this numerical study. Nonlinear force-based beam-column elements with fiber sections were used to model the RC walls. One element per story was used. The material models Concrete03 and Steel02 were used for confined concrete and steel, respectively [51]. The initial concrete modulus was $E_c$ = 35.2 GPa, while the concrete compressive strength $f_c'$ = 48 MPa. The confined concrete strength was $f_{cc}'$ = 68 MPa at a strain of 0.6%. The steel modulus, the yield stress, and the strain-hardening ratio were $E_s$ = 200 GPa, $F_y$ = 455 MPa, and $b$ = 0.02, respectively.

The first-story gravity columns and all slabs of the gravity framing system were modeled using *BeamWithHinges* elements [51], where a fiber section is defined for the plastic hinges, of length 0.91 and 0.41 m, respectively, at the ends of the element. The full width of 27.2 m of the slab was considered as effective. Horizontal rigid outrigger elements of length $L_w$ / 2 were used to model the length of the wall at each story, see Figure 8. The gravity columns for stories 2 to 20 were modeled with elastic elements with $I_e = 0.5I_g$.

Linear vertical, horizontal, and rotational zero-length springs were used to model the force-displacement behavior of the isolators in the corresponding degree of freedom. The vertical force, shear force, and bending moment interaction [52] were not considered in this study. The vertical stiffness of the isolators in tension was not modeled, since the BI and BIRW buildings were designed, so that the bearings do not undergo tension. Viscous dampers were modeled as zero length elements assigned a viscous material. The force-velocity nonlinear relationship of the dampers was $F = CV^a$ where $F$ is the force, $V$ the velocity, $C$, and $a$ constants. For the dampers used, the power factor $a$, was equal to 0.7 in all cases. For the 2000 kN vertical dampers at the rocking plane C was 4.4 MN·sec / m, while for the 1500 kN dampers C = 1.1 MN·sec / m. The slab, the core-wall, the columns, and the beams of the three underground

floors above the isolation plane were modeled with elastic beam-column elements of high axial and flexural rigidity.

The rocking plane was modeled with 17 zero-length springs, 8 representing effective area of the flange, 0.91 $m^2$ each, and 9 along the flange, 0.71 $m^2$ each. The stiffness of the contact springs was determined considering an element height equal to 0.3 m. The confined concrete material model with zero tensile strength was used to model these contact springs. The BRBs were modeled with truss elements using the steel material model described above. Rayleigh damping with 2% damping in the first and the third mode was used. A large deformation nonlinear response history analysis was conducted, with vertical mass modeled.

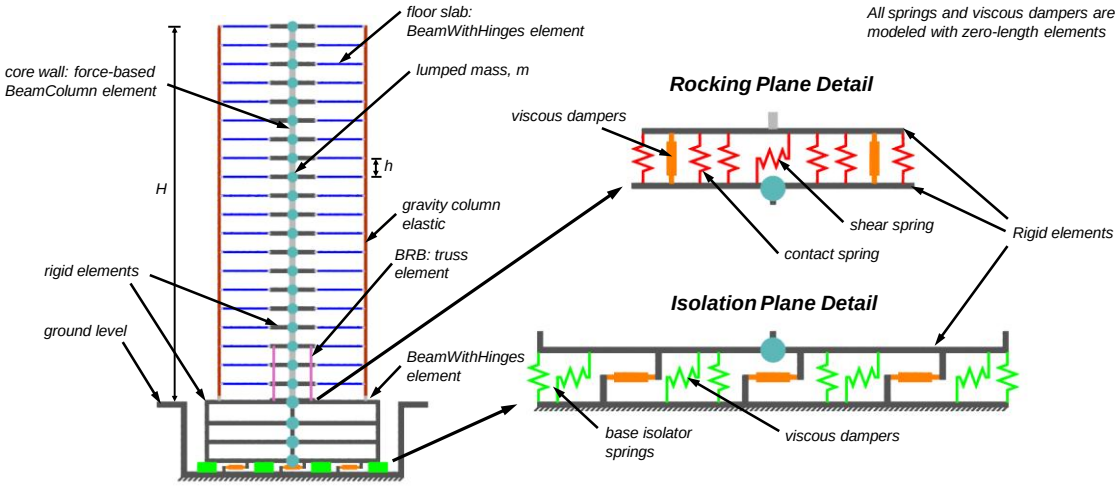


Figure 8. Elevation view of the numerical model with details of the isolation and rocking planes.

## 4 GROUND MOTIONS

Fourteen strong pulse-type near-fault ground motions from the Imperial Valley (1979), Loma Prieta (1989), Landers (1992), Northridge (1994), Kobe (1995), Chi-Chi (1999), and Duzce, Turkey (1999) earthquakes were used in this study. The elastic absolute acceleration and relative displacement spectra for 2% damping are presented in Figure 4. The ground motions were selected to have pulses of different predominant periods. Table 2 lists the predominant period of the pulses contained in these motions as well as the peak ground acceleration (PGA). The predominant periods of the pulses were calculated as the periods $T_{pi,Sv}$, and $T_{pi,Sa}$ at which the elastic velocity, and absolute acceleration spectra, respectively, had a distinct local peak.

As Table 2 shows, two or more distinct pulses with different predominant period were identified in most of the ground motions. As shown in Figure 4, the mean spectrum closely matches the MCE-level design spectrum between $T$ = 0.7 and 3.5 sec. The mean spectrum is close to the DBE-level in the constant acceleration period range. The MCE spectrum exceeds the mean spectrum for T larger than 3.5 sec. Individual motions included in the study (DUZCE, ELCEN6, LCN, TCU075, TCU102) exceed the MCE spectrum over different period ranges for $T$ larger than 3.5 sec.

The fourteen ground motions were divided in two sets of seven ground motions each. The first set, termed Short $T_p$, included the seven motions, for which the peak spectral velocity occurred for a $T_{pi,Sv}$ smaller than 2 sec. The second set, termed Long $T_p$, consisted of the seven ground motions, where the peak spectral velocity occurred for a $T_{pi,Sv}$ larger than 2 secs. Figure 4 also shows the mean acceleration and displacement spectra of the two sets. These graphs show that the mean acceleration spectrum of Set 1 exceeds the MCE-level design spectrum on average by 50% in the period range from $T$ = 0.6 to 2.5 sec, while the mean displacement spectrum of set 2 exceeds the MCE-level on average by 20% in the period range T = 2.5 to 7.0 sec.

Table 2. Characteristics of the fault-normal near-fault pulse-type ground motions used.

| | Record | Earthquake Location, Year | PGA (g) | $T_{p1,Sv}$ (sec) | $T_{p2,Sv}$ (sec) | $T_{p3,Sv}$ (sec) | $T_{p1,Sa}$ (sec) | $T_{p2,Sa}$ (sec) | $T_{p3,Sa}$ (sec) | $T_{p4,Sa}$ (sec) |
|---|---|---|---|---|---|---|---|---|---|---|
| Set 1 Short $T_p$ Ground Motions | LGP | Loma Prieta, CA, 1989 | 0.65 | 3.23 | 1.69 | 0.75 | 2.74 | 1.54 | 0.45 | - |
| | RRS | Northridge, CA, 1994 | 0.89 | 1.00 | - | - | 0.75 | - | - | - |
| | SCS | Northridge | 0.59 | 2.94 | 1.14 | - | 2.94 | 1.10 | - | - |
| | TAK | Kobe, Japan, 1995 | 0.68 | 2.09 | 1.29 | - | 1.94 | 1.24 | - | - |
| | TARZANA | Northridge | 1.33 | 4.38 | 2.09 | 0.70 | - | 2.09 | 0.70 | - |
| | TCU 084 | Chi-Chi, Taiwan, 1999 | 1.15 | 4.83 | 1.74 | 0.90 | - | - | 0.90 | 0.45 |
| | TCU 129 | Chi-Chi | 1.02 | 4.13 | 1.59 | - | - | - | 0.25 | - |
| Set 2 Long $T_p$ Ground Motions | DUZCE | Duzce, Turkey, 1999 | 0.36 | 5.62 | 0.80 | - | 5.22 | 0.80 | - | - |
| | ELCEN6 | Imperial Valley, CA, 1979 | 0.44 | 3.33 | - | - | 2.99 | - | - | - |
| | LCN | Landers, CA, 1992 | 0.77 | 4.13 | - | - | 4.03 | - | - | - |
| | TABAS | Tabas, Iran 1978 | 0.85 | 4.73 | 0.75 | - | 4.48 | 0.75 | - | - |
| | TCU 052 | Chi-Chi | 0.32 | 6.42 | 2.48 | - | 4.63 | 2.29 | - | - |
| | TCU 075 | Chi-Chi | 0.33 | 4.13 | - | - | - | - | - | - |
| | TCU 102 | Chi-Chi | 0.30 | 9.50 | 2.64 | - | - | 2.49 | - | - |

# 5 RESULTS OF NUMERICAL ANALYSIS

## 5.1 *Modal Analysis*

Table 3 presents the periods of the first three lateral modes ($T_{L,i}$), as well as the first vertical ($T_{V,1}$) of the buildings based on un-cracked concrete material properties. Base isolation increased the first and second mode of the fixed-base and RW buildings by 2.5 and 4.3 times, respectively. For the first three modes the normalized modal characteristics presented in Figure 9 are: (a) modal lateral force, (b) modal bending moment, and (c) modal shear force diagrams.

The normalized modal lateral force of mode $q$ at floor $i$, $r_{F,q,i} = F_{q,i} / (m_i \cdot A_q)$, is equal to the ratio of lateral force due to mode $q$, $F_{q,i}$, to the product of the modal acceleration, $A_q$, and the floor $i$ seismic mass, $m_i$. The normalized modal shear force, $r_{V,q,i} = V_{q,i} / (m_t \cdot A_q)$, is equal to the ratio of the shear force at floor $i$ due to mode $q$, $V_{q,i}$, to the product of the total seismic mass, $m_t$, times $A_q$. The normalized modal base shear force is equal to the effective modal mass, $m_q / m_t$. The normalized modal bending moment, $r_{M,q,i} = M_{q,i} / (m_t \cdot H \cdot A_q)$, is equal to the ratio of the bending moment at floor $i$ due to mode $q$, $M_{q,i}$, to $m_t$ times the height, $H$, of the building times $A_q$. Normalized modal shear forces at ground level for modes 1, 2, and 3 were 0.64, 0.18, and 0.07, respectively, for FB1, and 0.84, -0.01, and 0, respectively, for BI. The effective modal masses for modes 1, 2, and 3 were 0.64, 0.18, and 0.07 for FB1. The effective modal masses for

modes 1 and 2 for the BI building were 0.99 and 0.01, respectively, and practically 0 for mode 3. The modal characteristics indicate that use of base isolation significantly reduces the contribution of second and higher modes, and is expected to reduce forces and floor accelerations in the base isolated structures.

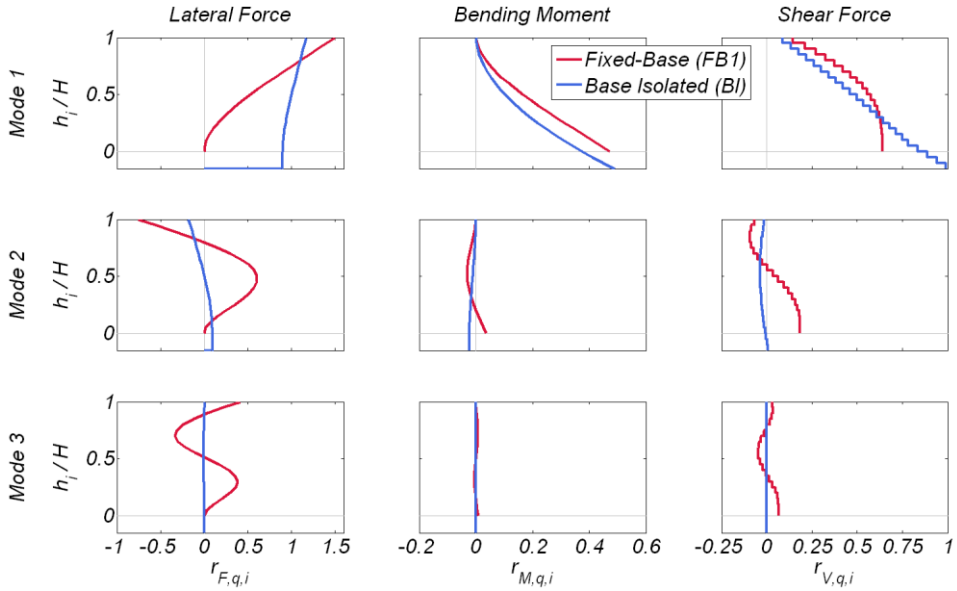


Figure 9. Modal characteristics of the FB1 and BI buildings.

Table 3. Modal periods (sec) of studied buildings.

| Mode | Fixed Base 1 (FB1) | Fixed Base 2 (FB2) | Base Isolated (BI) | Rocking Wall (RW) | BI and RW (BIRW) |
|---|---|---|---|---|---|
| $T_{L,1}$ | 1.59 | 1.55 | 3.79 | 1.55 | 3.79 |
| $T_{L,2}$ | 0.29 | 0.28 | 1.06 | 0.28 | 1.08 |
| $T_{L,3}$ | 0.17 | 0.17 | 0.24 | 0.17 | 0.24 |
| $T_{V,1}$ | 0.18 | 0.18 | 0.18 | 0.18 | 0.18 |

## 5.2 *Response History Analysis*

Figure 10 presents mean response envelopes of the buildings to the 14 near-fault ground motions. All the envelopes are presented in terms of the height, $h_i$, of floor $i$ from the ground level, normalized to the building height above ground, $H$. The presented responses are: the bending moment of the wall, $M$, normalized by the total building seismic weight above the ground level, $W$, times $H$; the tensile strain of bonded to concrete steel, $\varepsilon_s$, of the wall; the shear force of the wall, $V_i$, normalized by $W$; floor acceleration, $A$, normalized by the PGA; ratio of lateral displacement relative to the base of the building (different between isolated and non-isolated buildings), $D$, to $H$; and the interstory drift ratio, $\Theta$. Table 4 presents the mean values as well as the peak values, of different response parameters. The floor accelerations and shear forces presented are filtered with a finite impulse response (FIR) low-pass filter, of order 5000, with a 10 Hz cut off frequency [54].

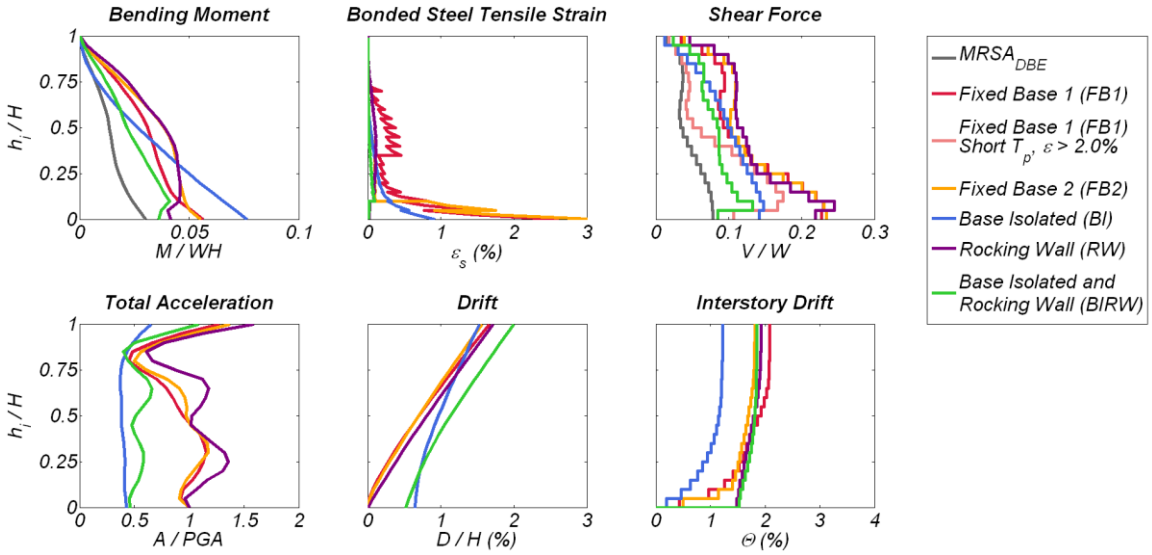


Figure 10.Mean response envelopes.

Corresponding to significant structural damage, significant inelastic deformations developed at the base of the fixed-base building with the mean and peak strains exceeding 2.6%, and 5.6%, respectively. In the FB1 building, inelastic deformations developed also around mid-height of the wall with the mean and peak tensile strains of 0.38% and 1.11%, respectively. The mean roof drift ratio of the FB1 and FB2 buildings was 1.7%, and 1.6%, respectively. The corresponding peak drift ratio was 3.9% and 3.6%, respectively. The mean, over the 14 motions, average along the height interstory drift of the fixed-base buildings exceeded 1.6%. The corresponding peak values were 3.6%. The response of the fixed-base buildings resulted in large base shear force with the mean, and peak to be 0.23*W*, and 0.33W, respectively.

The peak shear computed for FB2 corresponds to a shear stress of 6.5 MPa ($12.7\sqrt{f_c'}$ in psi where $f_c'$ = 7000 psi) in the core wall exceeding the maximum allowed by ACI [53]. This level of shear stresses with concurrent large values of inelastic strains crushing in the web of the core wall is a concern. The shear force envelope for instants where the tensile strain, at the ground level of the wall, is larger than 2% is also shown to indicate the level of shear forces under significant concurrent inelastic deformations. High floor accelerations were computed for both fixed-base buildings, with the mean average acceleration along the building height exceeding 0.91*PGA*.

In comparison with the FB buildings, the BI design resulted in significant reduction, of more than 40%, of the mean and peak shear forces and average floor accelerations while exhibiting similar roof drift ratios. As expected, and discussed above, the BI design was not able to prevent the formation of a flexural plastic hinge at the base of the core-wall above the ground level with the mean and peak tensile strain reaching 0.9% and 3.7%, respectively. The peak and mean displacements of the bearings were 0.43 m and 0.69 m, respectively.

The RW building experienced similar floor accelerations, forces, and displacements compared to the FB buildings. Compared to the FB building, the RW building prevented the formation of a plastic hinge at the base of the wall, with the mean and peak maximum strain in the bonded reinforcement being less than 0.14% and 0.31%, respectively. On its upper part, the RW building developed larger moments than the FB2 building. The mean uplift at the rocking plane of the wall was 0.12 m and the peak 0.25 m, with the corresponding rotation of the rocking plane equal to 1.5 rad and 3.2 rad, respectively. The mean and peak tensile strains of the BRBs were computed to be 1.6% and 3.3%, respectively.

As shown in Figure 10 and Table 4, the BIRW building was able to combine the beneficial effects of the base isolation plane, which reduced accelerations and lateral forces, and a rocking core-wall, which prevented plastic hinging and, thus, post-earthquake damage at the base of the wall, with the peak strain in the bonded tensile steel not exceeding 0.15%. Compared to the fixed-base designs, it reduced mean and peak shear forces more than 1.8 times, and the mean

average floor accelerations by 37%, while avoiding formation of a plastic hinge at the core-wall. Mean and peak displacements of the bearings were 0.35 and 0.46 m, respectively. Uplift at the rocking plane of the wall was 0.12 m and 0.31 m, respectively, corresponding to rotation of the rocking plane equal to 1.4 rad and 4.0 rad. The mean and peak strains of the BRBs were 1.6% and 4.1%, while the corresponding concrete compressive strains of the core-wall were 0.5% and 1.1%, respectively.

Table 4. Mean, and peak (in parenthesis) values of response parameters over 14 ground motions.

| | Fixed Base 1 (FB1) | Fixed Base 2 (FB2) | Base Isolated (BI) | Rocking Wall (RW) | BI and RW (BIRW) |
|---|---|---|---|---|---|
| Roof drift ratio, $D / H$ (%) | 1.7 (3.9) | 1.6 (3.6) | 1.5 (3.5) | 1.7 (3.4) | 2.0 (4.4) |
| Average interstory drift along the height, $\Theta_{avg}$ (%) | 1.7 (3.9) | 1.6 (3.6) | 0.9 (2.4) | 1.8 (3.4) | 1.5 (3.7) |
| Wall midheight bending moment, $M_{0.5H} / WH$ | 0.031 (0.045) | 0.039 (0.063) | 0.027 (0.042) | 0.039 (0.064) | 0.022 (0.028) |
| Wall ground level shear, $V / W$ | 0.23 (0.33) | 0.23 (0.33) | 0.12 (0.20) | 0.22 (0.34) | 0.10 (0.14) |
| Wall peak shear, $V / W$ | 0.25 (0.33) | 0.25 (0.37) | 0.15 (0.19) | 0.25 (0.38) | 0.14 (0.17) |
| Average acceleration along height, $A_{avg} / PGA$ | 0.91 (1.33) | 0.95 (1.46) | 0.42 (0.77) | 1.08 (1.61) | 0.57 (1.15) |
| Wall tensile strain in bonded steel, $\varepsilon_s$ (%) | 2.6 (5.6) | 3.0 (6.6) | 0.92 (3.7) | 0.14 (0.31) | 0.10 (0.15) |
| Concrete compressive strain at base of wall (%) | 0.17 (0.24) | 0.18 (0.27) | 0.13 (0.26) | 0.47 (0.89) | 0.47 (1.10) |
| BRB tensile strain (%) | - | - | - | 1.6 (3.3) | 1.6 (4.1) |
| Uplift of wall (m) | - | - | - | 0.12 (0.25) | 0.12 (0.31) |
| Wall rotation at 1st story (rad) | 0.007 (0.017) | 0.008 (0.020) | 0.004 (0.013) | 0.015 (0.032) | 0.015 (0.040) |
| Isolator displacement (m) | - | - | 0.43 (0.69) | - | 0.35 (0.46) |
| Gravity column tensile strain (%) | 0.15 (0.47) | 0.19 (0.60) | 0.04 (0.29) | 1.04 (2.45) | 1.09 (3.05) |
| Gravity column compressive strain (%) | 0.15 (0.25) | 0.16 (0.27) | 0.08 (0.20) | 0.37 (0.64) | 0.37 (0.81) |
| Ratio of moment resisted by gravity system to total, $M_G / M_{total}$ | 0.28 (0.33) | 0.28 (0.33) | 0.22 (0.24) | 0.37 (0.41) | 0.38 (0.41) |

Figure 11 presents the response envelopes to the 14 individual ground motions for the response parameters described above. The bending moment at the ground level for the buildings without an isolation plane was determined by the bending moment strength of the wall at this level as well as by the level of hardening it experienced. This is why small variation is observed in terms of base moment of the wall in the FB and RW buildings. A significantly larger

variation of ground level moment is observed for the BI building because some of the motions resulted in limited inelastic response at the base of the wall, while other motions resulted in inelastic response higher than the corresponding response of the FB buildings. As a result of the variation of the predominant period of the distinct pulses contained in the ground motions, significant variation in the shape of the bending moment envelope for the buildings without base isolation was observed.

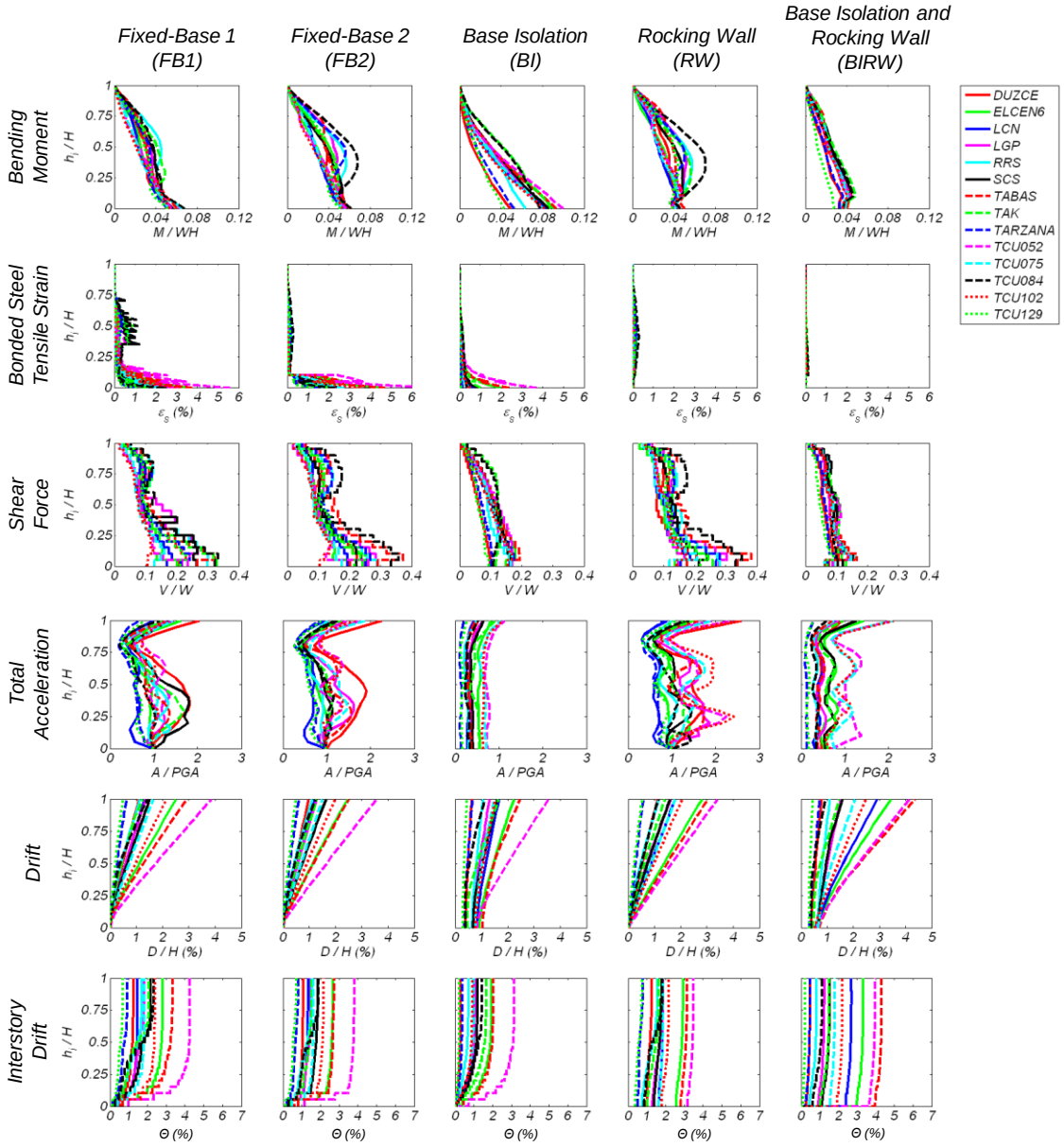


Figure 11. Response envelopes to individual ground motions of the five buildings.

The base-isolated buildings showed significantly smaller sensitivity to the frequency content of the ground motions in terms of shape of the bending moment envelope. A nearly linear bending moment envelope for all ground motions is noted, demonstrating the efficiency of base isolation in reducing the second and higher modes of response.

As noticed for the bending moment envelopes, the shear force envelopes followed the first mode shear force profile for BI and BIRW buildings, while for FB1, FB2, and RW buildings showed significant contribution of the second mode of response for some ground motions; see the local peak of shear force at 0.75*H*.

For floor accelerations, the BI was the only design that showed small sensitivity of the shape of the acceleration envelope to the ground motion characteristics. Acceleration envelopes of the BI were nearly constant over the height of the buildings for all 14 ground motions and below PGA. The FB and RW designs show the highest sensitivity while the BIRW design does show also some non-negligible sensitivity.

The displacement and interstory drift ratio envelopes for all buildings were dominated by the first mode of response. The peak roof displacement for all buildings except the BIRW occurred for the TCU052 motion. TABAS and ELCEN6 were the other two motions with highest displacement demand. As shown in Figure 4, these were the three motions with the highest $S_d$ for periods around 4 sec.

### 5.3 *Effect of Predominant Period of Pulses Contained in the Ground Motions*

Figure 12 depicts the mean envelopes of response of the FB1 and BIRW buildings separately for the two sets of seven ground motions used in this study. As expected, the ground motions with long-period pulses resulted in larger displacements compared to motions with short-period pulses.

The short-period motions (Set 1) resulted in 41% larger mean base shear force for the FB1 building than Set 2. The shear forces for the BIRW were similar for the two sets, indicating that base isolation effectively reduced second and higher mode effects. The motions with long-period pulses resulted in 65% larger bonded steel strain, than Set 1 at the base of the FB1 building, while the motions with short-period pulses resulted in 8.1 times larger (and equal to 0.68%) than Set 2 mean strains at the midheight of the FB1 building. The motions with long-period pulses resulted in 1.7 times larger normalized average floor accelerations in the BIRW building because for the long-period motions, the average PGA was 0.48 g, which was 1.9 times smaller than the average PGA of the motions with short-period pulses. The mean PGA of the seven short period and long period ground motions was 0.91 and 0.48 g, respectively.

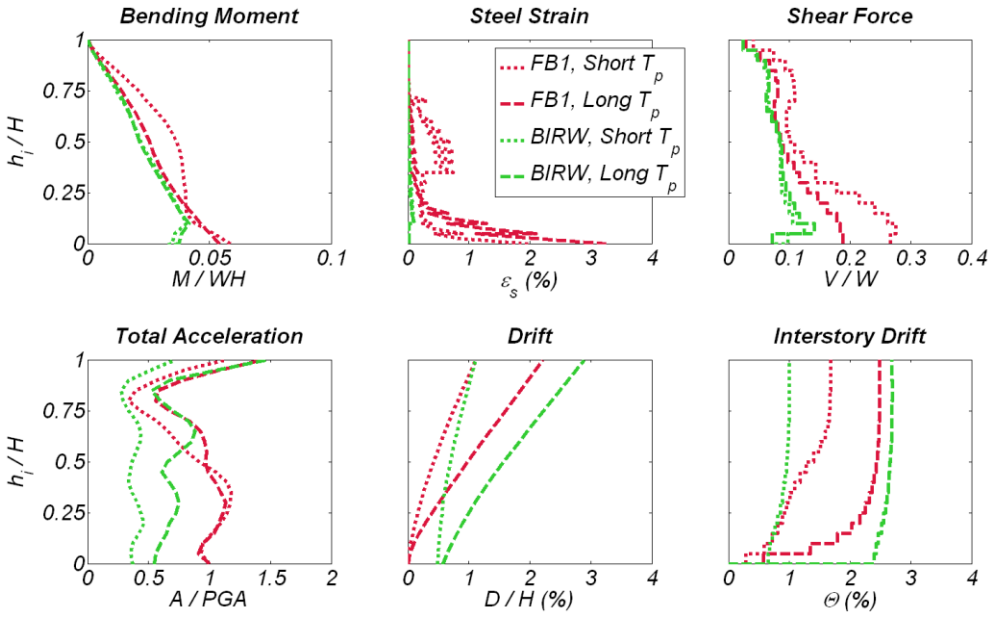


Figure 12.Mean envelopes of FB1 and BIRW for ground motions with pulses of "short" (Set 1) and "long" (Set 2) period ($T_p$).

### 5.4 *Effect of Amount of Hysteretic and Viscous Energy Dissipation at the Rocking Plane of BIRW Building*

This part of the study investigated the effect of hysteretic energy dissipation using the BRBs and the viscous energy dissipation using the vertical viscous dampers at the rocking plane of the BIRW building. Four variations of the BIRW building were compared. The first was the reference BIRW design (BIRW1), described above, which used eight BRBs and eight viscous dampers at the rocking plane. The second version, BIRW2, did not use vertical dampers, the third, BIRW3, did not use BRBs, while the fourth, BIRW4, used neither vertical viscous dampers nor BRBs. As shown in Table 5 and Figure 13, not using vertical viscous dampers resulted in less than 9% increase of mean and peak average accelerations along the height, while all the other response parameters increased by less than 5% in comparison with BIRW1.

The case of BIRW3 (without BRBs but with vertical viscous dampers) resulted in a 25% increase of both the mean and peak average floor acceleration in comparison with the reference BIRW building. The corresponding increases of the wall uplift were 25% and 23%, while the isolator displacement decreased by 9%, indicating that reducing the flexural static strength of the wall results in more of the deformation being accommodated by the rocking mechanism and less by the base isolation plane. The case of BIRW4 (the BIRW building with neither BRBs nor vertical dampers) resulted in the largest increase of floor accelerations and wall uplift between the four versions considered. In comparison with the reference BIRW building (BIRW1), BIRW4 resulted in 35% larger mean average floor accelerations and 42% larger wall uplift, while the average interstory drift along height was 33% larger.

Figure 14 plots the base moment versus first story rotation of the FB1 and BIRW1 to BIRW4 buildings. This plot shows the energy dissipation characteristics of the moment-rotation response of the buildings. The reduced strength of the BIRW buildings in comparison with the fixed-base resulted in increase of the wall rotation. As expected viscous damping did not increase significantly the peak moment strength.

Table 5. Mean, and peak (in parenthesis) values of response parameters over 14 ground motions for the rocking plane parameter study for BIRW building.

| | BIRW1 | BIRW2 | BIRW3 | BIRW4 |
|---|---|---|---|---|
| Rocking plane characteristics | Reference BIRW: 8 BRBs, 8 viscous dampers | 8 BRBs, No viscous dampers | No BRBs, 8 viscous dampers | No BRBs, No viscous dampers |
| Roof drift ratio, $D / H$ (%) | 2.0 (4.4) | 2.1 (4.7) | 2.2 (4.9) | 2.3 (5.3) |
| Average interstory drift along height, $\Theta_{avg}$ (%) | 1.5 (3.7) | 1.6 (4.0) | 1.8 (4.4) | 2.0 (4.8) |
| Wall shear force, $V / W$ | 0.14 (0.17) | 0.14 (0.18) | 0.13 (0.16) | 0.14 (0.17) |
| Average acceleration along height, $A_{avg}$ / PGA | 0.57 (1.15) | 0.62 (1.25) | 0.71 (1.44) | 0.77 (1.52) |
| Wall uplift (m) | 0.12 (0.31) | 0.13 (0.33) | 0.15 (0.38) | 0.17 (0.42) |
| Isolator displacement (m) | 0.35 (0.46) | 0.34 (0.43) | 0.32 (0.42) | 0.32 (0.41) |
| Damper force in rocking plane (kN) | 1316 (2127) | - | 1573 (2545) | - |
| Damper force in isolation plane (kN) | 1010 (1473) | 1011 (1483) | 1023 (1539) | 1040 (1556) |

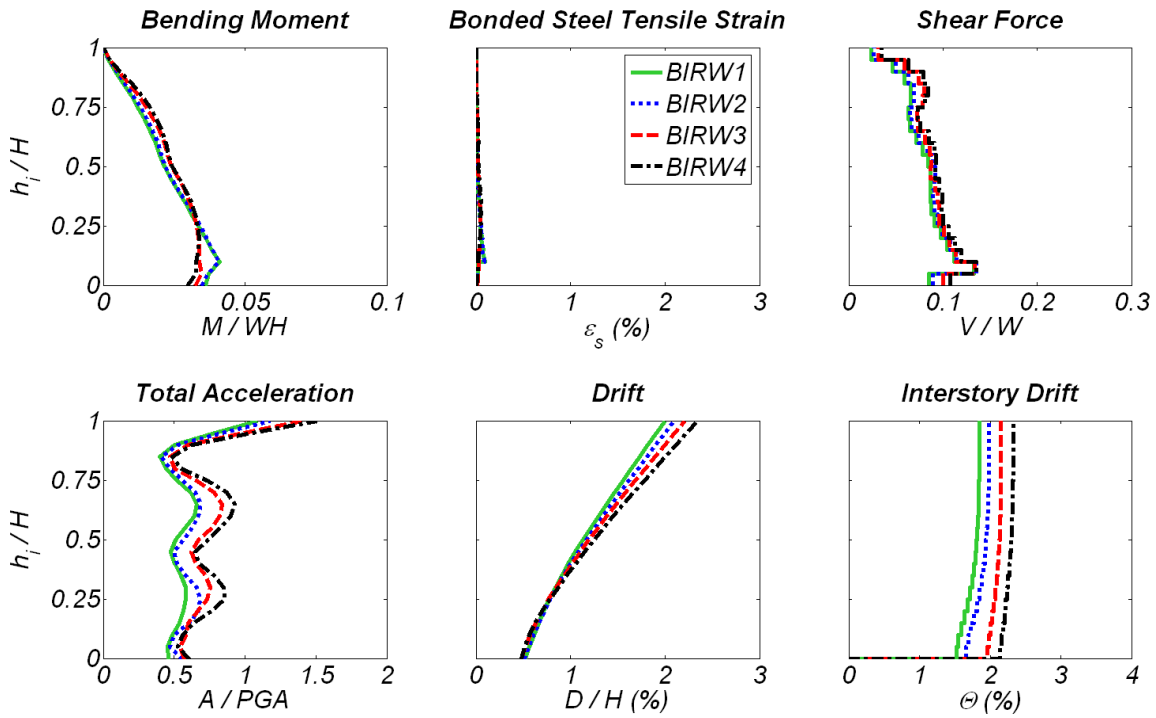


Figure 13. Effect of amount of hysteretic and viscous energy dissipation in the rocking plane of BIRW building.

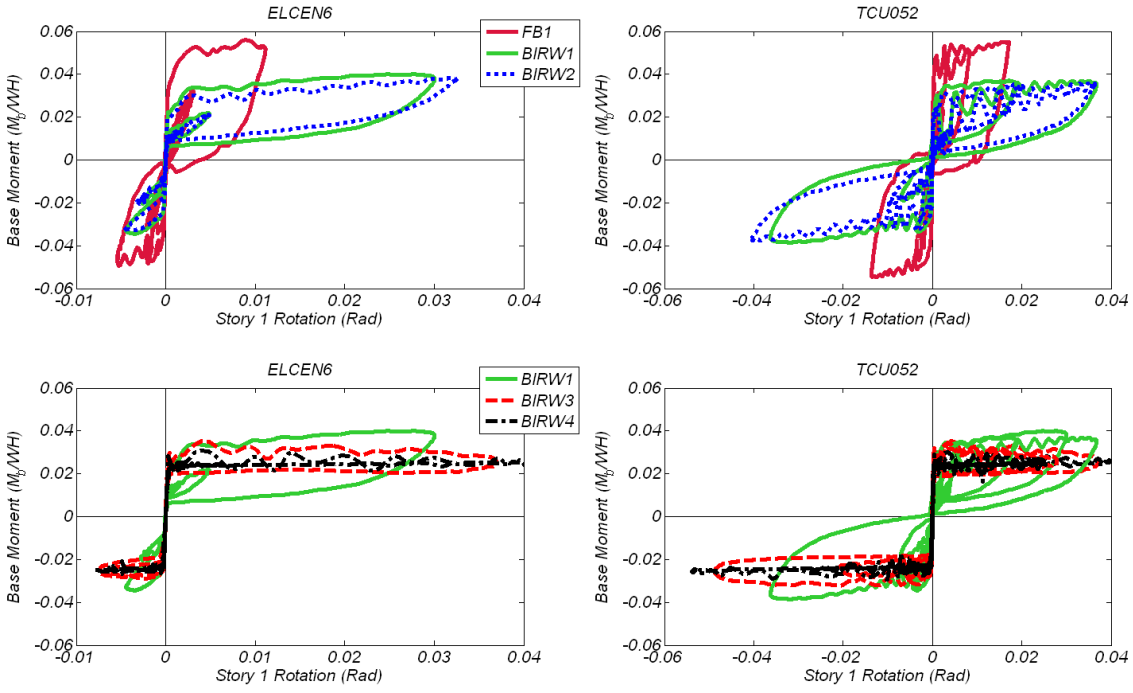


Figure 14. Base moment versus first story rotation of FB1 and BIRW1-4 buildings subjected to ELCEN6 and TCU052 ground motions.

5.5 *Effect of Amount of Viscous Energy Dissipation at the Isolation Plane of BIRW Building*

The effect of the amount of viscous energy dissipation at the base isolation plane was investigated for the BIRW building. In addition to BIRW1, which used twelve dampers of 1500 kN peak force capacity, the case of using half the amount of peak viscous damping force was considered in the BIRW5 building, which used twelve 750 KN dampers. The BIRW6 building used no viscous dampers in the isolation plane. As shown in Table 6, and Figure 15, viscous energy dissipation is very effective in reducing, primarily, displacement of the bearings, and, secondarily, of floor accelerations, relative displacements, wall uplift, and interstory drifts.

In comparison with BIRW1, the increases of mean displacements of the bearings, roof drift ratio, average interstory drift, and wall uplift in BIRW6 were 66%, 30%, 60%, and 50%, respectively. Note also that peak force of vertical dampers in BIRW6 is 1.46 times larger (which is larger than the capacity of the dampers considered) than the corresponding force in the BIRW1 building. A comparison of the mean responses of BIRW5 and BIRW1 indicates that doubling the amount of viscous damping resulted in 14%, 22%, 15%, and 19% decrease of average interstory drift, peak wall uplift, peak base shear force, and isolator displacement, respectively.

Table 6. Mean, and peak (in parenthesis) values of response parameters over 14 ground motions for the isolation plane parameter study.

| Name of building | BIRW1 | BIRW5 | BIRW6 |
|---|---|---|---|
| Number and force capacity (kN) of dampers | 12 / 1500 | 12 / 750 | 0 |
| Roof drift ratio, $D / H$ (%) | 2.0 (4.4) | 2.3 (4.6) | 2.6 (4.8) |
| Average interstory drift along height, $\Theta_{avg}$ (%) | 1.5 (3.7) | 1.9 (4.1) | 2.4 (4.5) |
| Wall uplift (m) | 0.12 (0.31) | 0.14 (0.34) | 0.18 (0.37) |
| Isolator displacement (m) | 0.35 (0.46) | 0.43 (0.53) | 0.58 (0.82) |
| Wall shear force, $V / W$ | 0.14 (0.17) | 0.14 (0.16) | 0.16 (0.21) |
| Average acceleration along height, $A_{avg}$ / PGA | 0.57 (1.15) | 0.63 (1.18) | 0.77 (1.42) |
| Damper force of rocking plane (kN) | 1316 (2127) | 1502 (1986) | 2005 (3100) |
| Damper force of isolation plane (kN) | 1010 (1473) | 577 (786) | - |

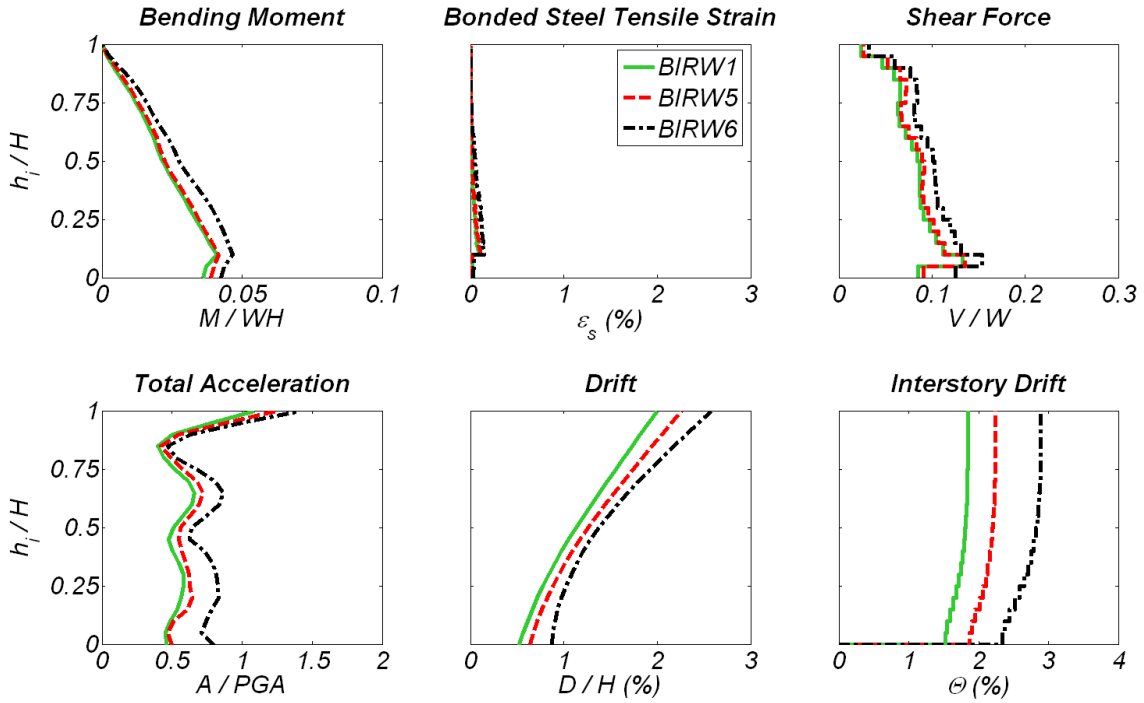


Figure 15. Effect of amount of viscous energy dissipation at the isolation plane of BIRW building.

Figure 16 plots the base moment versus first story rotation of the BIRW1, BIRW5, and BIRW6 buildings. Viscous damping reduced the peak first story rotation and peak base moment, while leading to a smoother response with fewer high frequency oscillations.

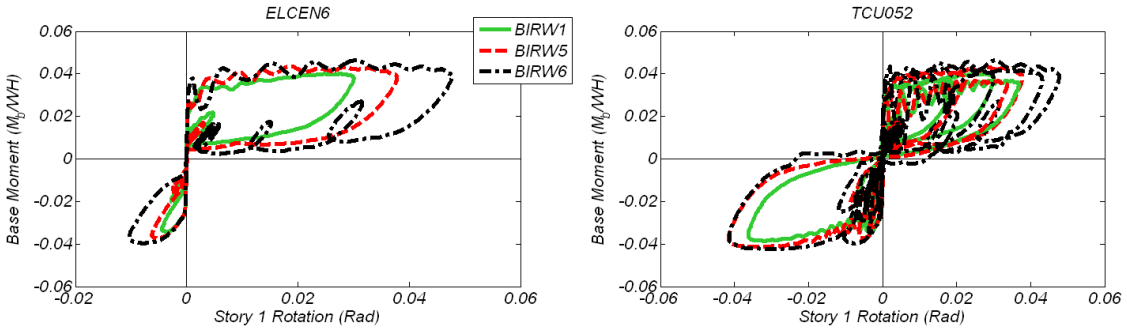


Figure 16. Base moment-rotation behavior for BIRW1, 5, and 6 subjected to ELCEN6 and TCU052 ground motions.

### 5.6 *Effect of Stiffness of Base Isolation Plane in BI Building*

The effect of stiffness of the base isolation plane of the BI building is investigated next. In addition to the reference BI building with 24 bearings (termed $BI_{24}$), three more BI buildings were considered with 36, 30, and 18 bearings, respectively. The individual bearings of all buildings, as well as the viscous dampers used, were identical. The longitudinal steel ratio in the core wall of all the buildings was 2.4%. As expected, mean and peak displacements of the bearings increased with a decrease in the stiffness of the isolation plane. The increase of the peak displacements was even greater in comparison with the corresponding increase of the mean displacements. In comparison with the reference BI building, neither the increase nor the decrease of the stiffness of the isolation plane was able to prevent inelastic response of the wall at the ground level. Average floor accelerations, drifts, and shear forces show small sensitivity to the stiffness of the isolation plane for the considered range.

Table 7. Mean, and peak (in parenthesis) values of response parameters over 14 ground motions for the BI isolation plane stiffness parameter study.

| Name of building | $BI_{36}$ | $BI_{30}$ | Reference BI ($BI_{24}$) | $BI_{18}$ |
|---|---|---|---|---|
| Number of bearings | 36 | 30 | 24 | 18 |
| Fundamental period (sec) | 3.2 | 3.4 | 3.8 | 4.3 |
| Isolator displacement (m) | 0.34 (0.46) | 0.38 (0.56) | 0.43 (0.69) | 0.49 (0.84) |
| Isolator compressive stress (MPa) | 4.9 (5.4) | 6.0 (6.8) | 7.2 (8.2) | 9.1 (10.5) |
| Bonded steel strain (%) | 1.3 (4.2) | 1.2 (4.1) | 0.9 (3.7) | 0.5 (2.1) |
| Wall shear force, $V / W$ | 0.17 (0.21) | 0.16 (0.19) | 0.15 (0.19) | 0.14 (0.19) |
| Average acceleration along height, $A_{avg}$ / PGA | 0.48 (0.95) | 0.45 (0.92) | 0.42 (0.77) | 0.39 (0.72) |
| Damper force (kN) | 1056 (1581) | 1082 (1502) | 1124 (1437) | 1177 (1474) |

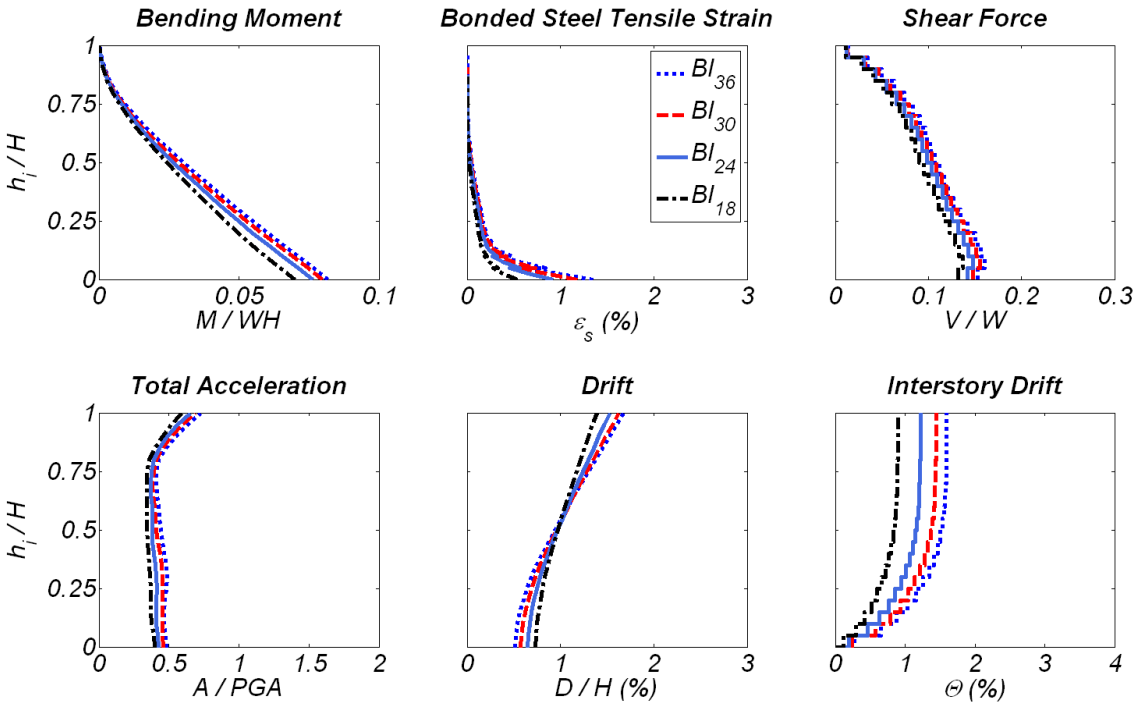


Figure 17. Effect of isolation plane stiffness in BI building.

## 6 SUMMARY AND CONCLUSIONS

This report investigated the use of base isolation and rocking core-wall designs to improve the seismic performance of tall RC core-wall buildings. Five 20-story RC wall buildings where considered. The first two buildings were conventionally designed to develop the majority of inelastic deformation in a flexural plastic hinge at the base of the core-wall. The third building used an isolation plane, consisting of elastomeric bearings, at the base of the building below the ground level. The fourth had a core-wall designed to rock at the ground level. A new design of a rocking core-wall cast in a steel shell over the first story height was proposed. Buckling restrained-braces and vertical viscous dampers were externally fastened to the wall at the rocking plane. The last building included both the isolation plane and the rocking core-wall of the third and fourth buildings, respectively. The response of these buildings subjected to 14 strong pulse-type near-fault ground motions was compared and the following conclusions were drawn:

1) The building that used both base isolation and a rocking core-wall (BIRW) had superior performance that avoided the formation of a plastic hinge at the base of the wall, resulting in 1.8 times smaller base shear force in the wall and 37% lower average floor accelerations in comparison with the fixed-base buildings. The mean and peak isolator displacements were 0.35 and 0.46 m, while the corresponding strains of the BRBs were 1.6 and 4.1%, respectively. Critical elements of this building were repairable and adaptable over its service life.
2) The building with a core-wall designed to rock at the ground level avoided the formation of a flexural plastic hinge at the base of the wall without reducing floor accelerations and forces when compared to fixed-base buildings.
3) The buildings with base isolation below ground developed about two times smaller mean, as well as peak, accelerations and base shear force in comparison with the fixed base buildings

but was not able to prevent the formation of a flexural plastic hinge at the ground level of the wall.

4) The BIRW building demonstrated less sensitivity to the ground motion characteristics in terms of the shape of the bending moment, shear force, and floor acceleration envelopes.
5) The use of viscous dampers at the base isolation plane of the BIRW effectively reduced–primarily–the displacement of the bearings and–secondarily–the interstory drifts, wall rotation, and floor acceleration.
6) In addition to buckling restrained devices, the use of vertical viscous dampers at the rocking plane did not result in significant reduction of the considered response parameters. The case of a rocking core-wall without BRBs and viscous dampers increased response quantities without resulting in overturn.

## REFERENCES


1. Council on Tall Buildings and the Urban Habitat (CTBUH). 2011. *Tall Building Database*. http://www.ctbuh.org/Resources/WorldsTallest/tabid/123/Default.aspx.
2. Otani, S. 1999. RC buildings damage statistics and SDF response with design seismic force. *Earthq. Spectra* 15(3):485–501.
3. Tsai, K.C., Hsiao, C.P., Bruneau, M. 2000. Overview of building damages in 921 Chi-Chi earthquake. *Earthq. Engrg. Engrg. Seismo.* 2(1):93–108.
4. Carpenter, L. D., Naeim, F., Lew, M., Youssef, N. F., Rojas, F., Saragoni, G. R., Schachter Adaros, M. 2011. Performance of tall buildings in Viña del Mar in the 27 February 2010 Offshore Maule, Chile, earthquake. *Struct. Design Tall Special Bldgs.* 20:17–36.
5. Lew, M., Naeim, F., Carpenter, L. D., Youssef, N. F., Rojas, F., Schachter Adaros, M., Saragoni, G. R. 2010. Seismological and tectonic setting of the 27 February 2010 Offshore Maule, Chile earthquake. *Struct. Design Tall Special Bldgs* 19:838–852.
6. Youssef, N. F., Tunick, D., Naeim, F., Lew, M., Carpenter, L. D., Rojas, F., Saragoni, G. R., Schachter Adaros, M. 2011. Performance of the Torre Bosquemar and Olas Buildings in San Pedro de la Paz and the Pedro de Valdivia Building in Concepción in the 27 February 2010 Offshore Maule, Chile, earthquake. *Struct. Design Tall Special Bldgs.* 20:65–82.
7. Rojas, F., Naeim, F., Lew, M., Carpenter, L. D., Youssef, N. F., Saragoni, G. R., Schachter Adaros, M. 2011. Performance of tall buildings in Concepción during the 27 February 2010 moment magnitude 8.8 Offshore Maule, Chile, earthquake. *Structural Design of Tall and Special Buildings* 20:37–64.
8. Kam, W.Y. 2011. Critically damaged multi-storey RC buildings. *Day 03 Field Report, Christchurch 22 Feb 2011 6.3Mw Earthquake.* http://www.eqclearinghouse.org/2011-02-22-christchurch.
9. U.S. Geological Survey. 2011. http://earthquake.usgs.gov/earthquakes/states/historical.php.
10. Celebi, M. 1992a. Highlights of Loma Prieta responses of four tall buildings. *Proceedings, Earthquake Engineering Tenth World Conference, Rotterdam, Holland.*
11. Celebi, M. 1992b. The Loma Prieta, California, earthquake of October 17, 1989 – building structures. *U.S. Geological Survey Professional Paper 1552-C.*
12. Naeim, F. 1994. Implications of the 1994 Northridge earthquake ground motions for the seismic design of tall buildings. *Struct. Design Tall Bldgs*3:247–267.
13. Naeim, F. 1998. Performance of 20 extensively-instrumented buildings during the 1994 Northridge earthquake. *Struct. Design Tall Bldgs.* 7:179–194.
14. International Code Council. 2009. *International Building Code.*
15. Lew, M. 2006. Design of tall buildings in high-seismic regions. *Struct. Design Tall Special Bldgs* 16:537–541.
16. Los Angeles Tall Buildings Structural Design Council. 2005. *An Alternative Procedure for Seismic Analysis and Design of Tall Buildings Located in the Los Angeles Region.*

17. Structural Engineers Association of Northern California. 2007. Seismic design and review of tall buildings using non-prescriptive procedures. *Recommended Administrative Bulletin, San Francisco*.
18. Willford, M., Whittaker, A., Klemencic, R. 2008. Recommendations for the seismic design of high-rise buildings. *Council on Tall Buildings and the Urban Habitat, Draft for Comment*, February 21, 2008; 28.
19. Moehle, J., Bozorgnia, Y., et al. 2011. Case studies of the seismic performance of tall buildings designed by alternative means. Task 12 report for the Tall Buildings Initiative. *PEER Report 2011/05*, University of California, Berkeley, CA.
20. Klemencic, R., Fry, A., Hooper, J.D., Morgen, B.G. 2007. Performance-based design of ductile concrete core wall buildings – issues to consider before detailed analysis. *Struct. Design Tall Special Bldgs* 16:599–614.
21. Panagiotou, M., Restrepo, J.I. 2009. Dual-plastic hinge design concept for reducing higher-mode effects on high-rise cantilever wall buildings. *Earthq. Engrg. Struct. Dyn.*, 38(12):1359–1380.
22. Calugaru, V., Panagiotou, M. 2011. Response of tall cantilever wall buildings to strong pulse-type seismic excitation. *Earthq. Engrg. Struct. Dyn.* DOI: 10.1002/eqe.1185.
23. Munir, A., Warnitchai, P. 2011. Optimal reduction of inelastic seismic demands in high-rise reinforced concrete core wall buildings using energy-dissipating devices. Published online, *Struct. Design Tall Special Bldgs.* DOI: 10.1002/tal.704.
24. Pan, P., Zamfirescu, D., Nakashima, M., Nakayasu, N., Kashiwa, H. 2005. Base-isolation design practice in Japan: introduction to the post-Kobe approach. *J. Earthq. Engrg.* 9(1):147–171.
25. Kani, N. 2009. Current state of seismic-isolation design. *J. Disaster Res.* 4(3):175–181.
26. Komuro, T., Nishikawa, Y., Kimura, Y., Isshiki, Y. 2005. Development and realization of base isolation system for high-rise buildings. *J. Advanced Concr. Tech.* 3(2):233–239.
27. Kawamura, S., Ogura, K., Tanaka, S., Yajima, A. 1998. Base and mid-story seismic isolation retrofit of middle rise RC buildings. *Proceedings, Second Japan-Turkey Workshop on Earthquake Engineering, Istanbul*; 383–394.
28. Ziyaeifar, M., Noguchi, H. 1998. Partial mass isolation in tall buildings. *Earthq. Engrg. Struct. Dyn..*, 27(1):49–65.
29. Tsuneki, Y., Torii, S., Murakami, K., Sueoka, T. 2009. Middle-story isolated structural system of high-rise building. *J. Disaster Res.* 4(3):229–238.
30. Calugaru, V., Panagiotou, M. 2010. Seismic isolation using single and dual shear hinging of tall cantilever wall buildings subjected to near fault ground motions. *Proceedings, 9th U.S. National and 10th Canadian Conference on Earthquake Engineering, Toronto*.
31. Calugaru, V., Panagiotou, M. 2011a. Seismic isolation of tall cantilever wall buildings using one or more isolation planes. *Proceedings, 8th International Conference on Urban Earthquake Engineering, March 7-8, 2011, Tokyo Institute of Technology, Tokyo*.
32. Chey, M.H., Chase, J.G., Mander, J.B., Carr, A.J. 2010. Semi-active tuned mass damper building systems: application. *Earthq. Engrg. Struct. Dyn.* 39(1):69–89.
33. Dynamic Isolation Systems (DIS). 2011. http://www.dis-inc.com/index.html.
34. Fujita, T. 1991. Seismic isolation rubber bearings for nuclear facilities. *Nuclear Engrg. Design* 127:379-391.
35. Muramatsu, Y., Nishikawa, I., Kawabata, I., Takayama, M., Kimura, Y. 2001. Tensile property of large-sized natural rubber bearing. *J. Arch. Bldg. Sci.* 116(1466):53–56.
36. Kato, R. 2003. The tensile tests of natural rubber bearings focused on the effect of the steel flange plates. *Proceedings, ASME Pressure Vessels and Piping Conference, Cleveland.*
37. THK. 2011. http://www.thk.com/us/products/class/sliderail/index.html
38. Earthquake Protection Systems (EPS). 2011. http://www.earthquakeprotection.com/.
39. Nielsen, G.M. 2009. Performance of rocking core walls in tall buildings subjected to severe seismic demands. *Master's Thesis*, University of California, Berkeley, CA.

40. Wiebe, L., and Christopoulos, C. 2009. Mitigation of higher mode effects in base-rocking systems by using multiple rocking sections. *J. Earthq. Engrg.* 13(1):83–108.
41. Vassiliou, M.F., Makris, N. 2011. Analysis of the rocking response of rigid blocks standing free on a seismically isolated base. *Earthq. Engrg. Struct. Dyn.*, DOI: 10.1002/eqe.1124.
42. American Society of Civil Engineers, 2006. *Minimum Design Loads for Buildings and Other Structures.* ASCE 7-05, Reston, VA.
43. Federal Emergency Management Agency (2000). *Prestandard and Commentary for the Seismic Rehabilitation of Buildings*, FEMA 356, Washington, D.C.
44. Holden T., Restrepo, J., Mander J. (2003). Seismic Performance of Precast Reinforced and Prestressed Concrete Walls. *ASCE Journal of Structural Engineering*, Vol. 129, No. 3.
45. Schoettler, M.J., Belleri, A., Zhang,D., Restrepo, J.I., Fleischman, R.B. 2009. Preliminary results of the shake-table testing for the development of a diaphragm seismic design methodology. *PCI Journal*, 54(1), pp. 100-124.
46. Restrepo, J.I., Rahman, A. 2007. Seismic performance of self-centering structural walls incorporating energy dissipaters. ASCE, *J. Struct. Engrg.*, 133(11):1560–1570.
47. Marriott, D., Pampanin, S., Bull, D.K., Palermo, A. 2008. Dynamic testing of precast, post-tensioned rocking wall systems with alternative dissipating solutions. *Bull. New Zealand Soc. Earthq. Engrg.* 41(2):90–102.
48. Newell, J., Uang, C., Benzoni, G. 2006. Subassemblage testing of CoreBrace buckling-restrained braces (G series). *Report No. TR-06/01*.Dept. Struct. Engrg., University of California, San Diego, CA.
49. Taylor Devices Inc. 2011. http://www.taylordevices.com/dampers-seismic-protection.html. Last accessed on 12/07/2011.
50. Kelly, J.M., Takhirov, S.M. 2004. Analytical and numerical study on buckling of elastomeric bearings with various shape factors. *Earthquake Engineering Research Center Report, UCB/EERC-2004/03*, University of California, Berkeley, CA.
51. Open System for Earthquake Engineering Simulation (OpenSees). 2011. opensees.berkeley.edu.
52. Ryan, K.L., Kelly, J.M., Chopra, A.K. 2005. Nonlinear model for lead–rubber bearings including axial-load effects. ASCE, *J. Engrg. Mech.*, 131(12):1270–1278.
53. American Concrete Institute. 2011. *Building Code Requirements for Structural Concrete (ACI 318-11) and Commentary*. ACI 318-11,ACI Committee 318, Farmington Hills.
54. Matlab Reference Guide. 2008. *The MathWorks, Inc.*, Natick, MA.